A wave-to-wire model for grid integration studies of oscillating-body wave energy converters

Paula B. Garcia-Rosa[1], Raymundo E. Torres-Olguin[1], Joao Cruz[2], Salvatore D'Arco[1]
[1] *SINTEF Energy Research*, Trondheim, Norway
[2] *Yavin Four Consultants*, Lisbon, Portugal
E-mails: paula.garcia-rosa@sintef.no, raymundo.torres-olguin@sintef.no,
joao.cruz@yavinfourconsultants.com, salvatore.darco@sintef.no

***Abstract*—Wave energy converters (WECs) are still at an earlier stage of development when compared to other variable renewable energy systems based on wind or solar power. Indeed, only a few WECs have exported power to electric grids until recently. Thus, the development of mathematical models able to represent essential aspects of the system and its connection to the grid becomes fundamental to assess the impact of integrating wave power to grids. This work develops a fully integrated wave-to-wire model, where an electrical model that has re-configurable dynamic models of rotary and linear generators (with controllers) to accommodate different types of oscillating-body systems is interfaced with the WEC hydrodynamic and mechanical models. A complete wave-to-grid model is presented by integrating the generator system model, an electrical grid interface unit and a network equivalent for the receiving grid in a unified simulation environment with the WEC-Sim, an open-source tool widely used for simulating the dynamic behaviour of WECs. Numerical simulation studies are presented considering different operating conditions for the grid integration of a floating body that is connected to either an hydraulic power take-off system or a direct-drive system.**

***Index Terms*—Wave energy, Wave-to-wire, Grid integration, Power electronics**

I. Introduction

To date, only a few wave energy converters (WECs) have delivered power to external grids. Examples of such devices include oscillating wave column (OWC) devices like the LIMPET on the Scottish island of Islay, the Oceanlinx demonstration tests in Australia, and the Pico Power Plant, which provided power to a regional grid in Portugal during many time intervals from 2000 to 2016 [1], [2]. Other examples are the Wave Dragon, which delivered electricity to the grid in Denmark during prototype tests [3], and WECs deployed at the EMEC wave test facility in Orkney, Scotland, e.g., the Pelamis, Oyster, and Penguin Wello Oy [4].

A number of numerical simulation studies have been performed aiming at studying different aspects of grid integration of wave power, such as energy storage systems (ESSs) for power smoothing, evaluation of integration effects in weak grids and control of power electronics [5]–[8]. However, as discussed in a recent review on the topic [9], most studies on grid integration aspects of WECs do not fully consider the hydrodynamic characteristics of the WECs in the wave-to-wire models. As with other variable renewable energy systems that involve several disciplines, there is a tendency of treating separately the aspects related to hydrodynamics and electrical engineering in wave energy research.

The objective of this work is to develop a fully integrated wave-to-wire model including an electrical grid interface and a network equivalent for the receiving electric grid. In addition, the model is intended for different types of oscillating bodies. To this end, the model of electrical systems - from the power take-off (PTO) to the electric grid - are developed and integrated with the WEC hydrodynamic and mechanical models. The electrical model is referred as PTO-grid interface model and consists of generic dynamic models of rotary and linear generators with controllers, an interface unit including power electronic front-end with controllers and a simplified electrical ESS, as well as an equivalent model of an electric grid. The complete wave-to-grid model will be of use in the testing phase of the Horizon 2020 IMPACT project, which proposes a dual hardware-in-the-loop testing platform for different types of WECs [10].

To illustrate the functionalities and possible applications, the PTO-grid interface model is integrated with the WEC-Sim tool [11], a state-of-the-art WEC simulation tool that solves the multi-body dynamics, including hydrodynamics and calculation of mooring and PTO forces [12]. WEC-Sim has been used in different applications, e.g., in [13] the power profiles obtained through the tool were used as input to PLEXOS for sizing of battery storage capacity and grid integration analysis. However, the aim in the present paper is to provide an extension to WEC hydrodynamic models, or simulation tools, by incorporating numerical models of electrical systems in an unified simulation environment. In such a way, relevant dynamics of the entire energy conversion process are considered from the incident waves to the grid connection, and relevant interactions can be depicted.

The remainder of this paper is organized as follows. Section II outlines the dynamic modelling of oscillating bodies considering two types of PTO systems: hydraulic and direct-drive. Section III and IV present the PTO-grid interface model including its characterization and main limitations. Section V presents numerical simulations including the integration with WEC-Sim models, and Section VI concludes the paper.

This project has received funding from the European Union's Horizon 2020 research and innovation programme under IMPACT grant agreement No 101007071.

This is the accepted version of a paper presented at 2022 IEEE 31st International Symposium on Industrial Electronics - ISIE
http://dx.doi.org/10.1109/ISIE51582.2022.9831637

II. Equation of motion of oscillating bodies

In contrast to wind energy, where three blades horizontal-axis wind turbines are a clear dominant configuration, wave energy systems have not yet converged to a standard design. A large number of different wave energy technologies have been developed worldwide displaying different ways to absorb energy from the ocean waves [14]. This paper focuses on the broad class of WECs known as oscillating bodies. In these WECs, rigid bodies typically move with waves and produce electrical power either directly by means of a linear generator or through intermediate mechanical and hydraulic machinery, depending on the type of PTO system.

Under the assumption of linear hydrodynamic theory, the motion of a floating body can be described by the superposition of the wave excitation force (f_e), radiation force (f_r), the force produced by the PTO mechanism (f_p), restoring forces, as well as mooring and viscous forces. For simplicity, mooring and viscous effects are neglected here and only vertical motion is considered. Then, the body motion can be expressed as:

$$m\ddot{x}(t) + Sx(t) = f_e(t) + f_r(t) + f_p(t)\,, \tag{1}$$

with the radiation force being given by [15]:

$$f_r(t) = m_r(\infty)\ddot{x}(t) + \int_0^t h_r(t-\tau)\,\dot{x}(\tau)\,d\tau\,, \tag{2}$$

which represents the force produced by waves generated by the oscillatory motion of the body, and the excitation force being given by:

$$f_e(t) = \int_{-\infty}^{\infty} h_e(t-\tau)\,\zeta(\tau)\,d\tau\,, \tag{3}$$

which represents the force due to the incident waves ζ. In (1)-(3), x is the vertical position of the body, m is the body mass, $m_r(\infty)$ is the infinite-frequency added mass coefficient defined with the asymptotic values of the added masses at infinite frequency, S is the buoyancy stiffness, the convolution term of (2) is known as fluid-memory model [16], and h_e is the inverse Fourier transform of the excitation force transfer function (TF). The hydrodynamic parameters of the floating body are commonly calculated via frequency-domain boundary element method (BEM) codes, such as WAMIT [17].

In deep water, wind-generated waves are usually categorized as a Gaussian stochastic process and approximated as a superposition of a finite number of sinusoidal waves from a wave spectrum $S(\omega_a)$ [18]:

$$\zeta(t) = \sum_{i=1}^{m} \sqrt{2S(\omega_{ai})\,\omega_{ai}}\cos(\omega_{ai}t + \phi_i)\,, \tag{4}$$

where ω_{ai} and ϕ_i are the angular frequency and random phase of the i-th wave component, respectively. The wave spectrum can be characterized by defining a sea state with a certain significant wave height H_s (in meters) and a peak period T_p (in seconds). In addition, different spectral formulations can be adopted for $S(\omega_a)$. In this paper, the JONSWAP spectrum is considered in the simulations. This spectral formulation is based on wave measurements carried out in the late 60's for a program known as the Joint North Sea Wave Project.

The PTO force f_p depends on the type of PTO system utilized for the wave energy conversion.

A. PTO force of a generic system

For studies focusing on hydrodynamic models only, it is usual to consider a generic PTO with a spring-damper model, with the force being defined as:

$$f_p(t) = -B_p\dot{x}(t) - S_p x(t)\,, \tag{5}$$

where B_p is the damping coefficient and S_p is the stiffness coefficient.

B. PTO force for an hydraulic system

This paper considers an hydraulic PTO with a double acting piston, high and low pressure accumulators and an hydraulic motor, as described in [19], [20]. The piston is activated by the body motion and injects pressurized fluid in the hydraulic system. Then, the motor is driven by the flow resulting from the pressure difference between the high and low pressure accumulators. The resulting PTO force is given by [20]:

$$f_p(t) = (p_A(t) - p_B(t))A_p\,, \tag{6}$$

where p_A and p_B are the pressures at upper and lower parts of the piston, respectively, and A_p is the piston area. The full dynamic model of the hydraulic PTO showing how the pressures and fluid flow are calculated is described in [19] and omitted here for brevity.

C. PTO force of a direct-drive system

In direct-drive PTO systems, the generator captures the wave power directly from the motion of the floating body without the use of intermediate fluids, as in systems with hydraulic or pneumatic machinery. In this paper, the velocity of the floating body drives a linear generator with stator in the WEC spar and magnets in the rigid body [19]. As the body moves, it changes the magnetic field surrounding the coils, generating electricity. Then, the PTO force applied to the body is the electromagnetic force of the generator. This force will be described in Section IV-A.

III. Characterization of the PTO-grid interface model

The PTO-grid interface model consists of a set of functional blocks representing the energy conversion process from the PTO electrical output to the receiving electric grid, as illustrated in Figure 1. The main functional blocks of the developed numerical model represent:

- Generic dynamic model of rotary and linear generator with controllers.
- A grid interface unit consisting of a model for a power electronic front-end with its controllers, and a simplified

This is the accepted version of a paper presented at 2022 IEEE 31st International Symposium on Industrial Electronics - ISIE
http://dx.doi.org/10.1109/ISIE51582.2022.9831637

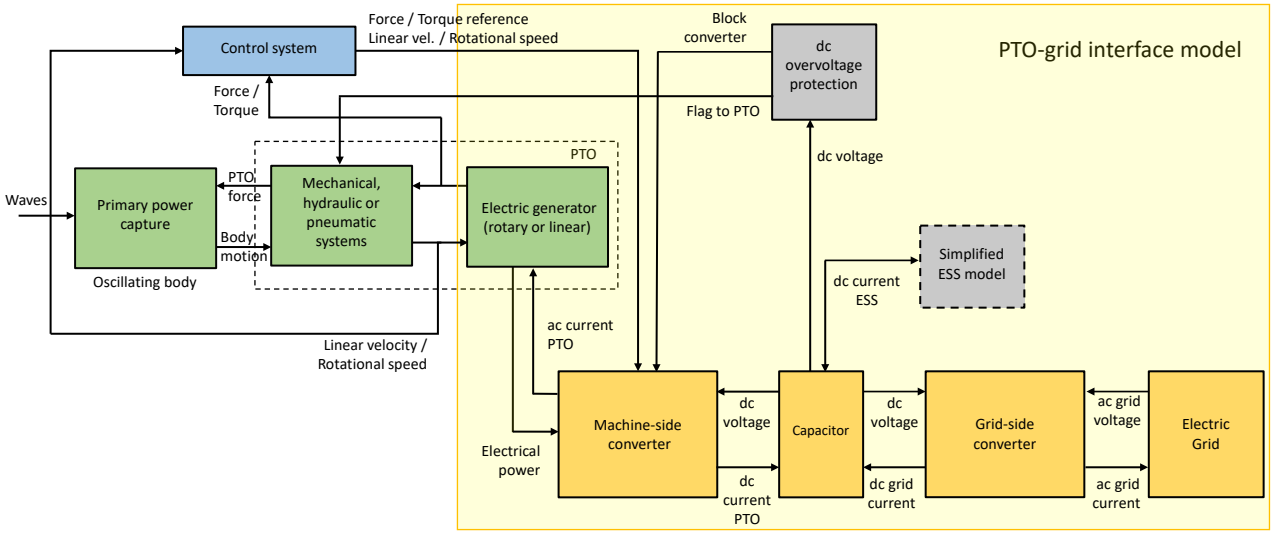

Fig. 1. Overview of a wave-to-wire model for oscillating bodies including grid interface and electric grid model. The main components of the PTO-grid interface model are highlighted.

model of an electrical energy storage device that can be optionally connected.

- A network equivalent model for the receiving electric grid.

A summary of the modelling approach for the PTO-grid interface model is presented in this section, including a brief overview of the inherent limitations of the models.

A. Electric generator and machine-side converter

The objective is to represent the main functionalities of an electric generator in a variety of oscillating body systems, regardless of the type of electric machine and drive utilized. Then, this block should represent a generic system, which inherently excludes representation of non-linear characteristics. The model is characterized by an efficiency gain plus a reduced-order transfer function that captures the most dominant modes of the electric machine dynamics and the drive system controlling the generator. As different types of PTO can be utilized for oscillating bodies, the generator model includes the implementation of speed, torque or force control. The machine-side converter operates as a controlled current source. The electrical power is calculated through a look-up table with machine speed and torque as inputs.

B. Electrical interface between PTO output and grid

A power electronic converter allows the WEC generator to operate at variable speeds by decoupling the rotor speed from the electrical frequency of the grid. A fully rated power electronics topology is adopted, as this is the most common topology in wave energy systems [9], [21]. The grid-side converter (GSC) is represented by an average model converter controlling the dc-link voltage and the reactive power injected into the grid through cascaded control loops. In this way, the model is computationally efficient as relatively large time steps can be used, e.g., 100 μs. However, it should be highlighted that while an average converter model is suitable for representing converter dynamics in power system studies, it cannot represent effects associated to the switching (e.g. ripple, high frequency harmonic distortion).

C. Electric grid

The grid is represented by a Thévenin equivalent circuit, i.e. a voltage source in series with an impedance, which is a general representation for every power system. Thus, different grid conditions can be conveniently emulated.

IV. PTO-GRID INTERFACE MODELLING

This section presents the models of the generator, the electrical interface unit and the electric grid.

A. Electric generator

Without loss of generality, we consider the electromagnetic equations of the permanent magnet synchronous generator (PMSG) in dq reference frame [22] to illustrate the derivation of the reduced-order transfer function. However, the simplified generic model is representative of any electric generator system following specific assumptions made with respect to the type of machine. For instance, for the PMSG it is assumed that the generator is operating below the field-weakening speed.

On this basis, the simplified drive structure is composed of a generic drive model which consists of a converter with current control, and a synchronous machine connected to a mechanical load. Fig. 2 illustrates the block diagram of the current control represented by decoupled PI current controllers in a synchronous dq reference frame. In Fig. 2, the power converter is approximated by a first-order transfer function with a time constant of T_0 seconds, v_s, i_s, R_s, and L_s represent the stator voltage, current, resistance, and inductance, respectively, the subscripts d, q represent d-axis and q-axis, k_{p0} and T_{i0} are the controller parameters, and s is the Laplace

This is the accepted version of a paper presented at 2022 IEEE 31st International Symposium on Industrial Electronics - ISIE
http://dx.doi.org/10.1109/ISIE51582.2022.9831637

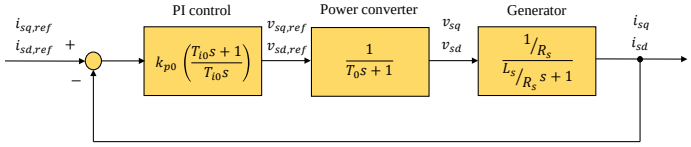

Fig. 2. Block diagram of a current controller for a generic drive system.

TABLE I
GENERATOR CONTROL IN OSCILLATING BODY WECS

Generator functionality:	**Generator control:**	**Examples: Oscillating bodies with**
Power conversion only	Constant speed control	Hydraulic PTO and accumulator smoothing
Optimization of prime mover efficiency	Variable speed or torque control	Variable speed hydraulic turbines
Device damping (direct influence on the body motion)	Torque control or force control	All-electrical or direct-drive PTOs

operator. For simplicity, the dynamic effect of T_0 is neglected, as it is much faster than the slow dynamics of the wave energy system. In addition, by setting the integral time constant to $T_{i0} = L_s/R_s$, there is a zero-pole cancellation as described in [23]. Then, the closed-loop transfer function for the block diagram in Fig. 2 becomes

$$G_{dq}(s) = \frac{k_{p0}}{sL_s + k_{p0}}\,. \tag{7}$$

By assuming that the PMSG is operating below the field weakening speed, the d-axis current i_{sd} is equal to zero [22], and (7) represents the closed-loop transfer function of the PI controller in the q-axis, which can be rewritten as:

$$G(s) = \frac{1}{sT_g + 1}\,, \tag{8}$$

where $T_g = K_{p0}^{-1} L_s$ is the time constant.

The current control in an electric machine is essential for manipulating the electromagnetic torque and magnetic flux. The electromagnetic torque for speeds below the field weakening is calculated as [22]:

$$T_e(t) = K_e i_{sq}(t)\,, \tag{9}$$

where K_e=1.5 $p\,\phi_f$, p is the generator pole pairs number and ϕ_f is the permanent magnet flux linkage. In addition, the machine speed is calculated from Newton's second law of motion:

$$\dot{\omega}_m = \frac{1}{J_m}(T_m - T_e - T_f)\,, \tag{10}$$

where T_m is the mechanical torque, T_f represents losses, and J_m is the combined inertia of the generator and mechanical load, e.g., a hydraulic motor in the PTO system.

For a linear generator, the current manipulates the electromagnetic force. In this case, it is assumed that the d-axis is aligned with the stator flux of the generator. By analogy with (9), the electromagnetic force can be calculated as [19]:

$$f_p(t) = k_m i_{sq}(t)\,, \tag{11}$$

where $k_m = \pi/\mu_m \phi_{fd}$, μ_m is the magnet pole pitch, and ϕ_{fd} is the stator d-axis flux linkage.

The reference for the current control can be obtained from either the torque or speed control system of rotary electric generators. For linear generators, the reference is obtained from the force control system. Table I summarizes the types of generator control commonly used in oscillating-body systems, as discussed in [24].

1) Torque control: The q-axis current is manipulated to obtain the desired torque reference $T_{e,ref}$. From (9),

$$i_{sq,ref} = k_e^{-1} T_{e,ref}\,, \tag{12}$$

where the reference is determined by a higher-level controller.

2) Speed control: It consists of a cascaded control where the outer loop is a PI controller regulating the machine speed and the inner loop is the current control (8). In this case, the current reference is calculated as:

$$i_{sq,ref} = -k_{pg}\left(\frac{sT_{ig}+1}{sT_{ig}}\right)\epsilon\,, \tag{13}$$

where $\epsilon = \omega_{m,ref} - \omega_m$ is the error signal, $\omega_{m,ref}$ is the machine speed reference, k_{pg} and T_{ig} are the speed controller parameters. The inner current control is much faster than the outer loop, as the dynamics of the outer loop are dictated by the mechanical system. Then, an ideal inner control loop is assumed for the purpose of tuning, and the parameters of the speed controller can be set as [25]:

$$k_{pg} = \omega_B^{sp} J_m\,, \quad T_{ig} = \frac{4}{\omega_B^{sp}}\,, \tag{14}$$

which should result in a critically damped transient response with reduced overshoot. Notice that the mechanical torque oscillations caused by the wave power oscillatory nature will have a significant effect in the system response. To avoid the amplification of such oscillations, the speed bandwidth frequency ω_B^{sp} is set to 10 rad/s in this work.

3) Force control: By analogy with (12), the current i_{sq} is obtained from the desired force reference $f_{p,ref}$. From (11):

$$i_{sq,ref} = K_m^{-1} f_{p,ref}\,, \tag{15}$$

and the force reference is determined by a higher-level controller, e.g., to optimize the wave energy absorption.

B. Electrical interface between PTO output and grid

1) Grid-side converter: The grid-side converter is responsible for regulating the dc-link voltage, which is required for the proper operation of the back-to-back voltage source converters (VSCs). The GSC is a three-phase VSC consisting of six IGBTs connected with free-wheeling diodes, as shown in Fig. 3. The VSC can be represented in the synchronous

This is the accepted version of a paper presented at 2022 IEEE 31st International Symposium on Industrial Electronics - ISIE
http://dx.doi.org/10.1109/ISIE51582.2022.9831637

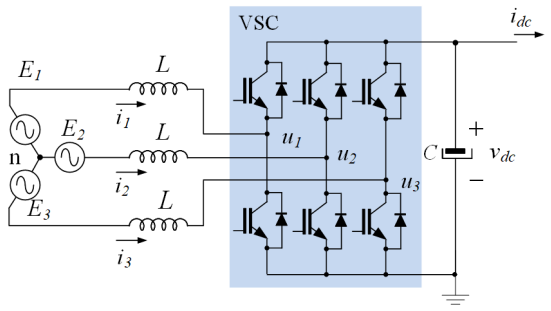

Fig. 3. Schematic of the grid-side voltage source converter.

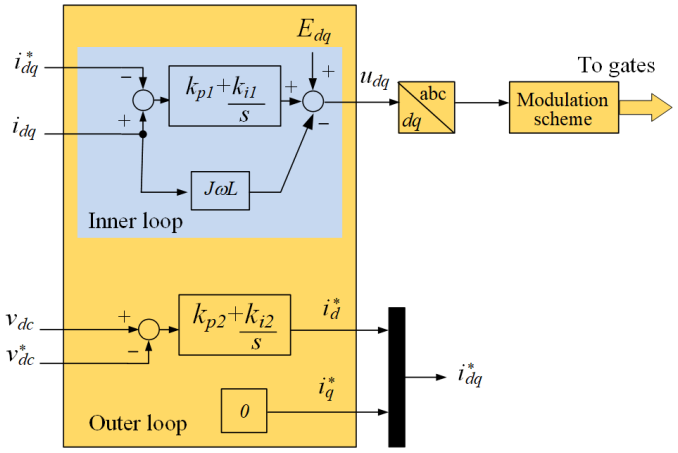

Fig. 4. Grid-side converter control.

reference frame using the well-known Park Transformation. The ac-side dynamics of the VSC is given by:

$$L\frac{d}{dt}i_{dq} = E_{dq} - u_{dq} - \omega L J i_{dq}\,, \tag{16}$$

where i_{dq}, E_{dq}, and u_{dq} represent, respectively, the ac current, ac voltage, and output voltage of the converter before the filter inductor in dq coordinates. Furthermore, ω is the angular frequency of the reference phase voltage, L is the sum of grid inductance and output filter inductance, and J is the anti-symmetric matrix, defined as

$$J = \begin{bmatrix} 0 & 1 \\ -1 & 1 \end{bmatrix}.$$

For the control system design, it is assumed that the dynamics of the inductors (16) are much faster than the dynamics of the capacitor at the dc link. Then, the control design is based on cascaded control loops where the inner loop is the current control and the outer loop is the voltage control.

The objective of the inner control loop is to guarantee that i_{dq} follows the reference i^*_{dq}. Following the dq-representation of the current dynamics (16), the output voltage reference u^*_{dq} is defined as:

$$u^*_{dq} = E_{dq} - \omega L J i_{dq} + \left(k_{p1} + \frac{k_{i1}}{s}\right)(i_{dq} - i^*_{dq})\,, \tag{17}$$

which includes the voltage E_{dq} and a cross-coupling term to eliminate the term $\omega L J i_{dq}$. The proportional and integral actions represented by gains k_{p1} and k_{i1} eliminate the steady-state error between i_{dq} and its reference i^*_{dq}. Fig. 4 shows a schematic of the inner loop. For simplicity, modulation delays are neglected and it is assumed that $u_{dq} = u^*_{dq}$.

The objective of the outer control loop is to regulate the dc voltage, which relies on the dynamics of the capacitor. From the power balance in the dc-link,

$$P_{cap} = P_{dc} - P_{ac}\,, \tag{18}$$

where P_{cap} is the power at the capacitor, P_{ac} is the power at the ac-side and P_{dc} is the power at the dc-side. The sign convention is indicated by Fig. 3. The power balance can be re-written in terms of voltages and currents to represent the dynamics at the dc-side:

$$C\frac{d}{dt}v_{dc} = i_{dc} - \frac{3E_d i^*_d}{2v_{dc}}\,, \tag{19}$$

where v_{dc} is the dc voltage at the capacitor and i_{dc} is the current from the WEC.

The dc voltage can be regulated through the current i_d by using the following PI controller:

$$i^*_d = \left(k_{p2} + \frac{k_{i2}}{s}\right)(v_{dc} - v^*_{dc})\,, \tag{20}$$

where k_{p2} and k_{i2} are the parameters of the outer PI control loop and v^*_{dc} is the dc voltage reference.

It should be noted that modelling electrical components in a synchronous reference frame is a common practice for both electrical drives and grid-connected converters. However, the orientation of the axes and the corresponding association of the d and q components to active and reactive power (magnetization) is traditionally different for such systems. More specifically, the active power is associated with the q component in motor drives and with the d component for grid-connected converters. Both conventions are also applied here to keep consistency with the literature.

2) Electrical energy storage: The ESS represents a simplified model of a battery-based system, which is emulated using a current source controlled by a PI controller. The reference for the battery controller is the power obtained after low-pass filtering the WEC output power. In this way, the battery smooths the power produced by the WEC, absorbing surplus or providing power when there is a power shortage. The ESS includes a simple state of charge (SOC) estimation based on Coulomb counting [26].

C. Electric grid

In this paper, the medium voltage and the distribution transformer are replaced by an equivalent voltage source. The equivalent impedance is an RL impedance, as the capacitance of the medium-voltage line is neglected. The strength of the grid is emulated by modifying the RL impedance, which can be described in terms of the short circuit ratio (SCR). The Thévenin impedance L_{TH} is calculated as follows:

$$L_{TH} = \frac{v_n^2}{2\pi f_n}\frac{1}{\mathrm{SCL}} = \frac{v_n^2}{2\pi f_n}\frac{1}{\mathrm{SCR}P_{wn}}\,, \tag{21}$$

This is the accepted version of a paper presented at 2022 IEEE 31st International Symposium on Industrial Electronics - ISIE
http://dx.doi.org/10.1109/ISIE51582.2022.9831637

where v_n represents the nominal voltage, SCL is the short-circuit level, and f_n is the nominal frequency. The SCL is calculated using the SCR and the nominal power of the WEC P_{wn}. The Thévenin resistance R_{TH} can be calculated by using the X/R ratio directly as

$$R_{TH} = \frac{2\pi f_n L_{TH}}{X/R}\,. \tag{22}$$

V. Numerical simulations

This section presents numerical simulations carried out with the full wave-to-wire model in MATLAB/Simulink. The PTO-grid interface models is integrated with the WEC-Sim tool, which solves the equation of motion of the body including the implementation of the PTO systems. The models of the electric generator (Section IV-A) are implemented in the WEC-Sim environment inside the *PTO-sim blocks* for each one of the PTO systems considered, and the grid-side models are implemented using the *Blocks Libraries* and the toolbox *Power Systems Blocks*.

The simulation models in the grid-side require a sampling frequency of at least 10 kHz for proper representation of the dynamic behavior. However, this sampling frequency is not necessary for representing the dynamics of the WEC-side models, and indeed make the computation time extremely slow. To transfer data between blocks operating at different rates, and to maintain the running time of the model to acceptable levels, the integration is performed by adding the block *Rate Transition*, as indicated by Fig. 5. This figure also shows a feedback through the variable "Flag to PTO" to illustrate the fault-ride through (FRT) capability of the generator. This flag informs the WEC to disconnect the PTO in case a grid fault is causing a voltage dip lower than the allowed limits and for longer time than an acceptable threshold (150 ms in this paper). Conversely, the generator must remain in operation.

A. Simulation parameters

The point absorber Reference Model 3 (RM3) available in the WEC-Sim library is utilized in the simulations. The RM3 is a two-body point absorber WEC with a floating part oscillating relative to a vertical column spar buoy. The WEC and its main dimensions are illustrated in Fig. 6. The input to the full wave-to-wire model is a sea state characterized by the JONSWAP spectrum. Two sea states are considered here, as defined in Table II. The main parameters of the PTO-grid models are shown Table III.

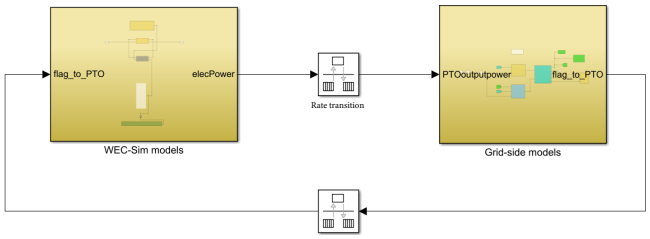

Fig. 5. Integration of WEC-Sim and grid-side models in MATLAB/Simulink.

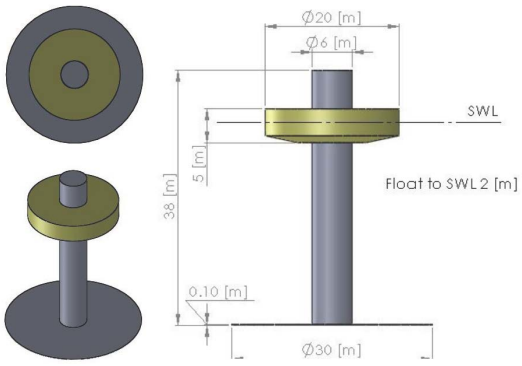

Fig. 6. Schematic of the point absorber RM3 [11].

B. Case studies

The case studies (CS) in this paper aim to show the main capabilities of the PTO-grid interface model and the integration with the WEC models. The point absorber RM3 is initially connected to a hydraulic PTO (CS1) and subsequently to a direct-drive PTO (CS2).

1) Grid connection of the RM3 with hydraulic PTO: Fig. 7 and Fig. 8 show the results of the CS1 from the incident waves to the active power exported to the grid, including the main variables of the WEC and grid-side models. In this case, the grid has strong characteristics (SCR=25) and the generator is operating with torque control, which is switched on 100 s after the simulation started and the mechanical system is at steady state. To minimize transients, and following usual requirements from grid codes, the power is initially exported as a ramp to the grid from 130 s. The aim of CS1 is to illustrate the behaviour of the integrated models when there is a fault condition in the grid causing a drop of 30% in the grid voltage from 140 s to 140.1 s. As the low-voltage operation lasts less than the specified threshold time, the WEC generator should remain connected to the grid, as indicated by the continuous

TABLE II
Sea states considered in the simulations.

Sea state	H_s (m)	T_p (s)
S1	3	8
S2	3.5	10

TABLE III
Main parameters of the PTO-grid interface models.

Parameter	Value	Unit	Description
T_g	15 (10)	ms	Current control time constant for the rotary (linear) generator
k_e	10.8	Nm/A	TF gain between torque and current
k_m	$\pi/0.009$	N/A	TF gain between force and current
f_n	50	Hz	Nominal frequency
v_n,V_{ac}	800, 400	V	Nominal dc and ac voltages
P_{wn}	100	kW	Nominal WEC power
X/R	7	-	Reactance and resistance ratio

This is the accepted version of a paper presented at 2022 IEEE 31st International Symposium on Industrial Electronics - ISIE
http://dx.doi.org/10.1109/ISIE51582.2022.9831637

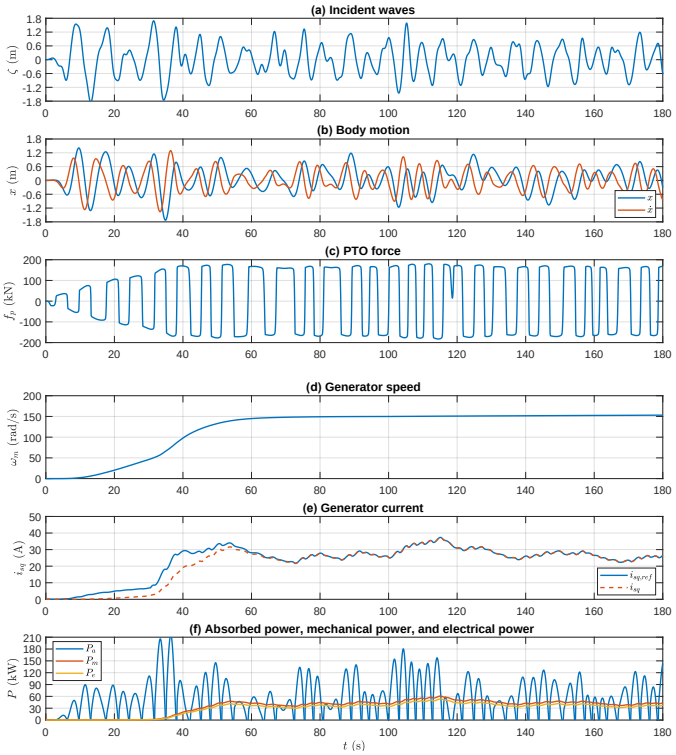

Fig. 7. Simulation results: Timeseries of WEC-side variables (CS1).

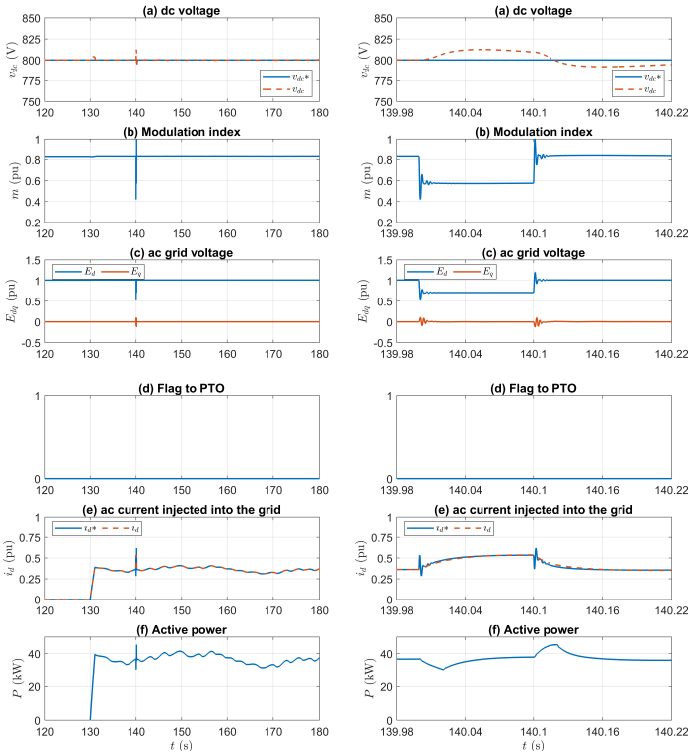

Fig. 8. Simulation results: Timeseries of grid-side variables (CS1). Left: 120 to 180s; Right: Zoom in transient period from 139.98 to 140.22 s.

operation of the generator in Fig. 7.d, and by the variable "Flag to PTO" in Fig. 8.d. The left side of Fig. 8 shows the results from 120 s to 180 s, while the right-side zooms in the time interval from 139.98 s to 140.22 s to better illustrate the transient behaviour. It can be observed that the voltage drop causes an increase in the d-axis currents (Fig. 8.e) and small oscillations in the dc voltage (Fig. 8.a) during a short-time transient, but it returns to the nominal value afterwards.

2) Grid connection of the RM3 with direct-drive PTO: As in previous case, the power produced by the WEC is initially exported as a ramp at 130 s. The CS2 illustrates the integrated models when the full system is under normal operating conditions and the WEC is connected to a weak grid (SCR=5) through an interface that either does not include an ESS (Fig. 10 at the left) or includes a simplified ESS (Fig. 10 at the right). Fig. 9 shows the main variables of the WEC-side models. In this case, the generator is operating with force control with reference defined by (5). The plot of the PTO force is omitted here, as the force is proportional to the generator current. For the case without ESS, the power exported is highly oscillatory, as the direct-drive PTO does not have any short-term energy storage capabilities as the hydraulic PTO does. Then, an impact on the grid is observed, as can be seen in the oscillatory behaviour of the dc voltage and ac grid voltage. Conversely, the use of a battery illustrates how the produced power from the WEC can be smoothed before being delivered to the grid. As a result, the impact on the grid is not significant. Although the grid has weak characteristics, the injected power of the WEC is small compared to its rated power. Notice that in the grid model, the rated power of the WEC is used for calculating the grid impedance, as expressed by (21).

VI. Conclusions

A fully integrated wave-to-wire model was presented for studying the grid connection of oscillating-body systems. A model representing the dynamics from the electric machine to a receiving grid was developed and integrated with hydrodynamic and mechanical models of the WEC. In such a way, relevant dynamics of the entire energy conversion process are considered and relevant interactions can be depicted.

Numerical simulation results were presented to illustrate the model functionalities and possible applications. The case studies are representative of normal operation and operation under the most common abnormal conditions in the grid. The results have confirmed that the model behaves as expected and that the running time is compatible with the needs for practical use.

The model of the electric machine and drive system are represented as a reduced order transfer function to easily accommodate different types of PTOs. As this is a generic model, non-linear characteristics which are specific to the types of machine are not well represented. In addition, the grid-side converter is represented by an average model converter which is suitable for representing converter dynamics in power system studies, but not suitable for representing effects associated to the switching, such as ripple and high frequency harmonic distortion.

This is the accepted version of a paper presented at 2022 IEEE 31st International Symposium on Industrial Electronics - ISIE
http://dx.doi.org/10.1109/ISIE51582.2022.9831637

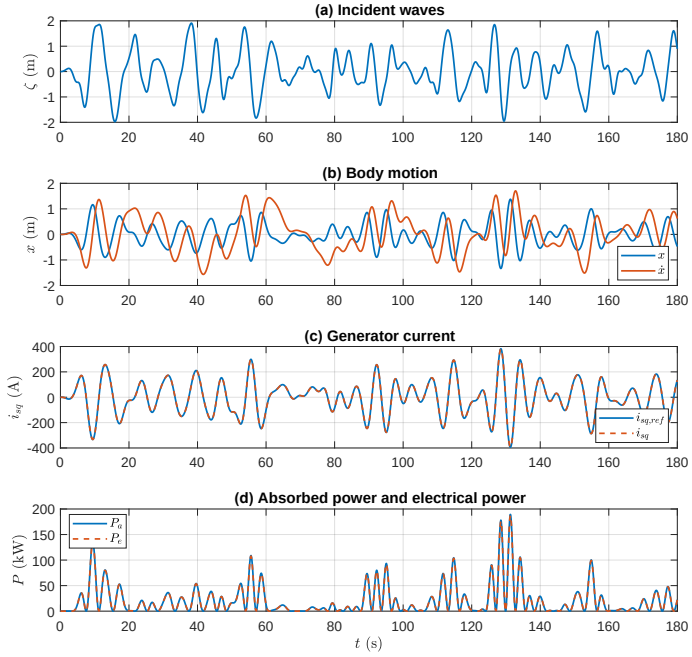

Fig. 9. Simulation results: Timeseries of WEC-side variables (CS2).

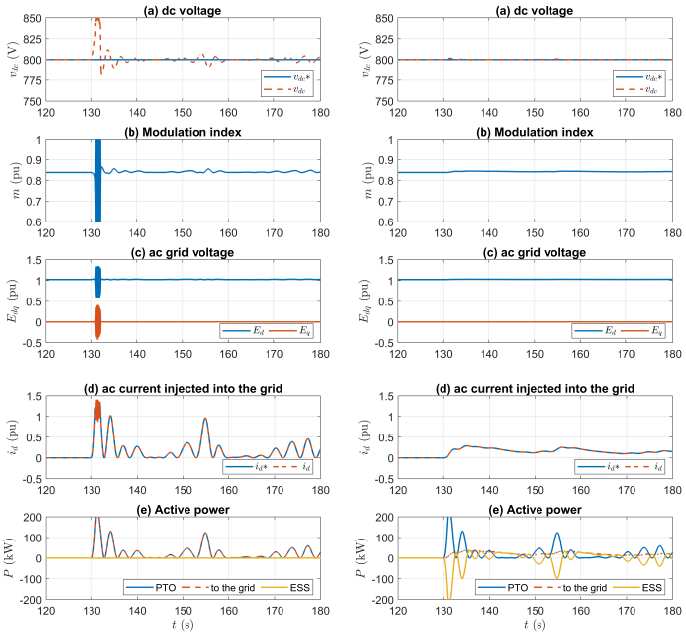

Fig. 10. Simulation results: Timeseries of grid-side variables (CS2). Left: The ESS is not connected to the electrical interface; Right: The ESS is connected.

REFERENCES

[1] T. V. Heath, "A review of oscillating water columns," *Philos. Trans. R. Soc. A Math. Phys. Eng. Sci.*, vol. 370, no. 1959, pp. 235–245, 2012.

[2] WaVEC. OWC Pico power plant. Acessed: 14.03.2022. [Online]. Available: http://www.pico-owc.net/en/.

[3] W. Dragon. Wave Dragon principles. Acessed: 14.03.2022. [Online]. Available: http://www.wavedragon.net/.

[4] EMEC. EMEC grid-connected wave test site. Acessed: 14.03.2022. [Online]. Available: https://www.emec.org.uk/facilities/wave-test-site/.

[5] F. Wu, X.-P. Zhang, P. Ju, and M. J. H. Sterling, "Modeling and control of AWS-based wave energy conversion system integrated into power grid," *IEEE Trans. on Power Sys.*, vol. 23, no. 3, pp. 1196–1204, 2008.

[6] F. Wu, P. Ju, X.-P. Zhang, C. Qin, G. J. Peng, H. Huang, and J. Fang, "Modeling, control strategy, and power conditioning for direct-drive wave energy conversion to operate with power grid," *Proc. of the IEEE*, vol. 101, no. 4, pp. 925–941, 2013.

[7] P. B. Garcia-Rosa, J. P. V. S. Cunha, F. Lizarralde, S. F. Estefen, I. R. Machado, and E. H. Watanabe, "Wave-to-wire model and energy storage analysis of an ocean wave energy hyperbaric converter," *IEEE Journal of Oceanic Engineering*, vol. 39, no. 2, pp. 386–397, 2014.

[8] S. Jafarishiadeh, M. Farasat, and S. Mehraeen, "Grid-connected operation of direct-drive wave energy converter by using HVDC line and undersea storage system," in *2017 IEEE Energy Conversion Congress and Exposition (ECCE)*, 2017, pp. 5565–5571.

[9] H. A. Said and J. V. Ringwood, "Grid integration aspects of wave energy - Overview and perspectives," *IET Renewable Power Generation*, vol. 15, no. 14, pp. 3045–3064, 2021.

[10] IMPACT project. Next-generation wave energy testing. Acessed: 14.03.2022. [Online]. Available: https://www.impact-h2020.eu/.

[11] K. Ruehl, D. Ogden, Y.-H. Yu, A. Keester, N. Tom, D. Forbush, and J. Leon, "WEC-Sim v4.4," 2021. [Online]. Available: https://zenodo.org/badge/latestdoi/20451353

[12] D. Ogden, K. Ruehl, Y. H. Yu, A. Keester, D. Forbush, J. Leon, and N. Tom, "Review of WEC-Sim development and applications," in *Proc. of the 14th European Wave and Tidal Energy Conf. (EWTEC)*, Plymouth, UK, 2021.

[13] J. Stefek, D. Bain, Y.-H. Yu, D. Jenne, and G. Stark, "Analysis on the influence of an energy storage system and its impact to the grid for a wave energy converter," in *Proc. of the ASME 38th Int. Conf. on Ocean, Offshore Mechanics and Arctic Eng.*, 2019, v010T09A031.

[14] A. F. O. Falcão, "Phase control through load control of oscillating-body wave energy converters with hydraulic PTO system," *Ocean Engineering*, vol. 35, no. 3, pp. 358–366, 2008.

[15] W. E. Cummins, "The impulse response function and ship motions," *Schiffstechnik*, vol. 47, no. 9, pp. 101–109, 1962.

[16] T. Perez and T. I. Fossen, "A Matlab toolbox for parametric identification of radiation-force models of ships and offshore structures," *Modeling, Identification and Control*, vol. 30, no. 1, pp. 1–15, 2009.

[17] WAMIT, Inc., *WAMIT User Manual Versions 6.4, 6.4PC and 6.3S, 6.3S-PC*, USA, 1998-2006.

[18] M. K. Ochi, *Ocean waves: The stochastic approach*. USA: Cambridge ocean technology series 6, Cambridge Univ. Press, 1998.

[19] R. So, A. Simmons, T. Brekken, K. Ruehl, and C. Michelen, "Development of PTO-Sim: A power performance module for the open-source wave energy converter code WEC-Sim," in *Proc. of the ASME 34th Int. Conf. on Offshore Mechanics and Arctic Eng. (OMAE)*, St. John's, Newfoundland, Canada, 2015, v009T09A032.

[20] A. F. O. Falcão, "Modelling and control of oscillating-body wave energy converters with hydraulic power take-off and gas accumulator," *Ocean Engineering*, vol. 34, pp. 2021–2032, 2007.

[21] I. López, J. Andreu, S. Ceballos, I. Martínez de Alegría, and I. Kortabarria, "Review of wave energy technologies and the necessary power-equipment," *Renewable and Sustainable Energy Reviews*, vol. 27, pp. 413–434, 2013.

[22] N. Mohan, *Advanced electric drives: analysis, control, and modeling using MATLAB/Simulink*. John wiley & sons, 2014.

[23] J. Sjolte, C. M. Sandvik, E. Tedeschi, and M. Molinas, "Exploring the potential for increased production from the wave energy converter Lifesaver by reactive control," *Energies*, vol. 6, no. 8, pp. 3706–3733, 2013.

[24] D. O'Sullivan, J. Bard, P. Kracht, S. Ceballos, and E. Robles, "Electrical generators in ocean energy converters," in *Electrical Design for Ocean Wave and Tidal Energy Systems*, R. Alcorn and D. O'Sullivan, Eds. London, UK: The Inst. of Eng. and Tech., 2013, pp. 3–41.

[25] R. W. De Doncker, D. W. J. Pulle, and A. Veltman, *Advanced electrical drives: analysis, modeling, control*. Netherlands: Springer, 2020.

[26] L. He and D. Guo, "An improved Coulomb counting approach based on numerical iteration for SOC estimation with real-time error correction ability," *IEEE Access*, vol. 7, pp. 74 274–74 282, 2019.

This is the accepted version of a paper presented at 2022 IEEE 31st International Symposium on Industrial Electronics - ISIE
http://dx.doi.org/10.1109/ISIE51582.2022.9831637